Biophysical Journal, Volume *110*

Supplemental Information

Kinetics of Formation and Asymmetrical Distribution of Hsp104-Bound Protein Aggregates in Yeast

Camille Paoletti, Sophie Quintin, Audrey Matifas, and Gilles Charvin

Kinetics of formation and segregation bias of Hsp104-bound protein aggregates in single dividing yeast cells

C. Paoletti, S. Quintin, A. Matifas, and G. Charvin

Supporting information & supporting figures

Text S1. Extended experimental procedures and model description

Strain List

Name	MAT	Background	Genotype	Origin
YCP03-1	a	S288C	*his3Δ1 leu2Δ0 lys2Δ0 met15Δ0 ura3Δ0 HSP104-GFP-HIS3MX6 CDC10-mCherry-kanMX4*	This study
YCP09-1	a	S288C	*his3Δ1 leu2Δ0 lys2Δ0 met15Δ0 ura3Δ0 HSP104-GFP-HIS3MX6 CDC10-mCherry-kanMX4 bni1Δ-KanMX4*	This study
YCP21-7D	a	S288C	*his3Δ1 leu2Δ0 lys2Δ0 met15Δ0 ura3Δ0 HSP104-GFP-HIS3MX6 HTB2-mCherry-kanMX4*	This study
YCP19-8D	a	Mix S288C / SEY6210	*HSP104-GFP-MX6 VPH1-mCherry-TRP1*	This study
YSQ01-A	a	YLL026W	*HSP104-GFP; 2μ pGAL1p-Ubc* 9^{ts}*-mCherry*	This study

Maintenance of focus during heat-shock experiments

All microscope parts and the sample holder undergo significant dilatation as the temperature is changed. This phenomenon has important implications for the maintenance of focus during rapid temperature changes. By using a Definite Focus (Zeiss) system to maintain a constant distance between the objective and the chip, we observed a drift of the focal plane by up to 23 μm during an abrupt temperature switch (TS) (Fig. S1C). Therefore, we combined the Definite Focus system hardware with homemade MATLAB software to maintain a constant distance between the objective and the chip, thereby allowing cells to be monitored during the TS.

Computational model of protein aggregation in dividing cells

The purpose of the computational model is to investigate whether the establishment of PA concentration asymmetry during the budded period of the cell cycle can be explained using a limited set of physical arguments. Therefore, hypotheses are included in the model in a sequential manner in order to understand the role of each specific feature.

Principle of the model

To model the aggregation kinetics of misfolded proteins into large protein clusters, we used the numerical framework described by [1] and later used by [2] to evaluate the distribution of PAs in fission yeast. In brief, the simulation is based on an exact stochastic simulation that derives from the Gillespie algorithm and models all possible reactions between the different species (i.e., PAs of different sizes). To this end, the simulation uses an aggregation kernel K(i,j) [3] that quantifies the frequency of collision between PAs of radius a_i and a_j:

$$\text{Frequency of aggregation} = K(i,j)\, N(i)\, N(j) \qquad \text{(Eq. 1)}$$

where N(i) and N(j) are the number of aggregates of radius a_i and a_j, and $K(i,j) = \frac{4\pi}{V}\left(D_i + D_j\right)(ai + aj)$, where D_i and D_j are the diffusion coefficients of particles of size a_i and a_j respectively [4], and V is the volume of the compartment.

We set N particles at the beginning of the simulation and we let the population of aggregates evolve due to fusion (and nucleation, see below) events that stochastically occur according to the Gillespie algorithm. Upon fusion of particles of size a_i and a_j, a new particle of size $\left({a_i}^3 + {a_j}^3\right)^{1/3}$ is generated, and the number of particles of size a_i and a_j decreases by 1. For each simulation step, as the number of aggregates evolves, the kinetic constants associated with aggregation of each particle are recomputed. This algorithm is iterated until all particles are aggregated or until the total duration reaches a set value (usually 200 min).

A major advantage of this framework is that it bypasses the need to simulate the spatial diffusion and collision of aggregates, which is computationally intensive because the two processes occur over very different timescales for particles of varying sizes.

A - Aggregation frequency

If we assume that aggregates follow the Stokes-Einstein equation: $D_i = \frac{k_B T}{6\,\pi\,\mu\,a_i}$

where k_B is the Boltzmann constant, T is the temperature, V is the volume of the compartment, and μ is the viscosity of the medium, then the aggregation kernel K can be rewritten as:

$$K(i,j) = \frac{2\,k_B\,T}{3\,V\,\mu}\left(a_i + a_j\right)\left({a_i}^{-1} + {a_j}^{-1}\right) \qquad \text{(Eq. 2)}$$

This is known as the Smoluchowski equation for coalescence of Brownian particles. An important feature of this formula is that only the ratio of particle size a_i/a_j is important for determining the order of magnitude of the aggregation kinetics. Therefore, no absolute size scale related to particle size appears in this formula.

By measuring the diffusion coefficient of particles of various sizes using mean square displacement analysis at different times following the TS (using mean square displacement analysis in confocal microscopy), we found that $D_i = \frac{\beta}{a_i^{\gamma}}$ yields the best fit with $\beta = 1.4 \times 10^{-4}$ and $\gamma = -2.1$, thus ruling out the hypothesis that PAs behave according to the Stokes-Einstein equation (Fig. S4). Therefore, by making the approximation that $\gamma \sim -2$, the aggregation kernel used in the simulation becomes:

$$K(i,j) = \frac{4\pi\beta}{V}\left(a_i + a_j\right)\left(a_i^{-2} + a_j^{-2}\right) \quad \text{(Eq. 3)}$$

Therefore, Eq. 3 features an absolute size scale for aggregating particles. Since there is conservation of the total volume of particles within aggregates, and N is the initial number of particles, the size of the initial particles is set to $a_1 = a_{max}/N^{1/3}$, where the maximum size of an aggregate a_{max} can be deduced from experiments: $a_{max} \sim 0.6$ μm (Fig. S4). Therefore, the kernel can be rewritten as:

$$K(i,j) = k\left((m_i/N)^{1/3} + (m_j/N)^{1/3}\right)\left((m_i/N)^{-2/3} + (m_j/N)^{-2/3}\right)$$

where m_i and m_j are the volumes of particles i and j ($1 < m_i < N$), and $k = \frac{4\pi\beta}{V\, a_{max}}$. Assuming V = 50 μm^3 (mean cell volume of yeast cells) yields k = 3.5 10^{-3} min^{-1}.

Fig. S5A shows the evolution of the number of aggregates with time resulting from the simulation described above, starting with a number N = 1000 particles. As expected, the kinetics of aggregation greatly depends on the aggregation rate k (colored lines on Fig. S5A). Importantly, the theoretical value k = 3.5 10^{-3} min^{-1} calculated from Eq. 3 provides a decent fit with the decay in aggregate number observed in the experimental data, even though it tends to underestimate the number of aggregates on timescales of >30 min (black line on Fig. S5A).

B- Initial number of particles

Since the maximal size of the largest aggregate is set to a constant value a_{max}, changing the number of initial particles N only affects the size of the initial particles: $a_1 = a_{max}/N^{1/3}$. Therefore, we expect this parameter to have no influence on the kinetics of aggregate fusion on long timescales. Indeed, using N between 50 and 5000, we saw no significant change in the kinetics of aggregation (Fig. S6B). Interestingly, this implies that the aggregation process is independent of the initial particle size and therefore of the nature of the proteins involved in the aggregation.

C- Aggregate visibility threshold

Our experiments showed that the number of visible aggregates increased during the first 20 min after the TS and then decreased to ~1/cell as they fused into larger structures (see Fig. 2 in the main text).

This non-monotonous variation in the aggregate number occurs because small aggregates formed immediately after the TS were too dim and/or diffused too rapidly to be detected experimentally.

To include this feature in the model, we introduced a visibility threshold T ($0 < T < 1$) so that any aggregate of volume smaller than T a_{max}^3 was invisible (Coelho et al. 2014). As expected, both the timing and the peak number of aggregates greatly depended on T (Fig. S6C), and higher T tended to decrease the height of the peak in the kinetics of aggregation.

T can be viewed as the volume ratio of the smallest detectable aggregate to the largest observed aggregate. We found that T ~0.1 provided the best agreement with the experimental data (Fig. S6C), suggesting that foci fluorescence intensity by the end of the aggregation process should be no more than 10 times that of the smallest foci (detected before or during the TS). However, our experiments directly contradicted this, yielding a ~100-fold difference in foci intensity before and after the TS (Fig. 1C in the main text), suggesting that an additional factor was setting the shape of the experimental aggregation kinetics, as described below.

D - Kinetics of formation of misfolded proteins

In addition to the kinetics of aggregate number described above, we focused on the PA concentration within cells as a function of time. We found that the experimental kinetics of aggregate accumulation was very different from that observed in the simulation. By the time the aggregate number peaked (red dashed line in Fig. S5D, E), <10% of the final PA fluorescence concentration had been reached experimentally (black curve) versus >75% in the simulation (green curve).

This delay in the accumulation of PAs could not be attributed to the time for Hsp104-GFP protein maturation, since they were already present upon TS. Up to this point in the simulation, we have considered that misfolded proteins were all generated at the time of the TS. However, the observation that the kinetics of aggregate number and fluorescence differed experimentally suggests that the kinetics of protein misfolding – rather than the kinetics of aggregate emergence above the visibility threshold due to particle fusion – may set the timescale for aggregate accumulation. Therefore, we modelled this using zeroth-order kinetics of formation of misfolded proteins, the rate k_m of which decays exponentially with time (per unit of volume) as follows:

$$k_m = k_0 \, e^{-\alpha t}$$

where k_0 is the initial rate of formation and α sets the timescale for the decay in misfolded protein formation. This requires only one additional parameter, since k_0 and α are linked to the total number of misfolded proteins N by:

$$N = \int_0^\infty k_m \, V \, dt \approx \; k_0 \, V/\alpha$$

assuming a constant volume during the course of the experiment. By fitting an exponential curve to the fluorescence accumulation kinetics (gray dashed line in Fig. S5E), we obtained $\alpha = 0.011$ min^{-1}

and we input this parameter in the simulation. As expected, the simulation accurately reproduced the experimental data for both aggregate concentration (Fig. S5E) and number (Fig. S5D). The agreement of the simulation with the experimental data was quite sensitive to the value of α, indicating that this parameter describes an essential feature of the aggregation kinetics.

The experimental kinetics of aggregate number was also captured well by the simulation, in which each parameter was either determined by the fit to experimental data or was derived from theoretical considerations —see below.

E- Parameter values

Parameter name	Value	Comment
a_{max}	0.6 μm	Maximal radius of aggregates;
k	3.5 10^{-3} min^{-1}	Aggregation frequency; estimated in section A above, knowing cell volume V and a_{max}
T	0.01	Aggregate visibility threshold (section C above); estimated from the ~100-fold difference in foci intensity before and after the TS (Fig.1C)
α	0.011 min^{-1}	Decay rate for the formation of unfolded proteins following TS (section D above); obtained by fit to the experimental data (Fig. S5E)
N	1000	Total number of aggregated proteins during the assay (section D). This arbitrary parameter sets the magnitude of the aggregation process, yet it plays no role in the aggregation kinetics (See Fig. S5B).

F- Effect of cell size and growth on aggregation kinetics

Having investigated the agreement between the model and the experimental aggregation kinetics using data obtained for mother cells, we wondered whether the model would predict the aggregation kinetics in buds, which have smaller and more variable initial volumes (typically V ~1–30 μm^3).

Interestingly, the evolution of the aggregate number in buds was in good agreement with the experimental data; the number of particles as a function of time was greatly modified in smaller compartments (Fig. 3F). This is due to the fact that the mean size of aggregates is smaller in smaller cells, which makes them more likely to fall below the visibility threshold T.

However, the aggregate concentration in the bud seems to be independent of the bud size, which contradicts the experimental data (with the exception of tiny buds, see Fig. 3E). This apparent contradiction is a consequence of maintaining a constant bud size throughout the simulation. By taking bud growth into account (as observed in Fig. 2G), we could recapitulate the kinetics of PA concentration (see main text and Fig. 3A–C).

Additional Bibliography

[1] Laurenzi, I.J., Bartels, J.D., and Diamond, S.L. (2002). A general algorithm for exact simulation of multicomponent aggregation processes. J Comp Phys *177*, 418–449.

[2] Coelho, M., Lade, S.J., Alberti, S., Gross, T., and Tolić, I.M. (2014). Fusion of protein aggregates facilitates asymmetric damage segregation. PLoS Biol *12*, e1001886.

[3] Hidy G.M., Brock, J.R. (1972). Topics in current aerosol research, Pergamon press.

[4] Friedlander, Sheldon K. (2000). Smoke, dust, and haze: fundamentals of aerosol dynamics, Oxford University Press.

Movie legends

Movie S1. Refers to Fig. 1. Cells undergoing the temperature shift from 30°C to 38°C at t = 2 h. Overlay of phase contrast and Hsp104-GFP (green) images. Scale bar: 4 μm.

Movie S2. Refers to Fig. 2. Differential accumulation of protein aggregates in mothers and buds for initially small-budded cells upon temperature shift from 30°C to 38°C at t = 2 h. The fluorescence signal corresponds to Hsp104-GFP. Lines represent cell and foci contours. Scale bar: 4 μm

Movie S3. Refers to Fig. 4. Nucleation of protein aggregates in daughter cells grown at 38°C over multiple generations. The fluorescence signal corresponds to Hsp104-GFP. Lines represent cell and foci contours. Scale bar: 4 μm

Supporting figures

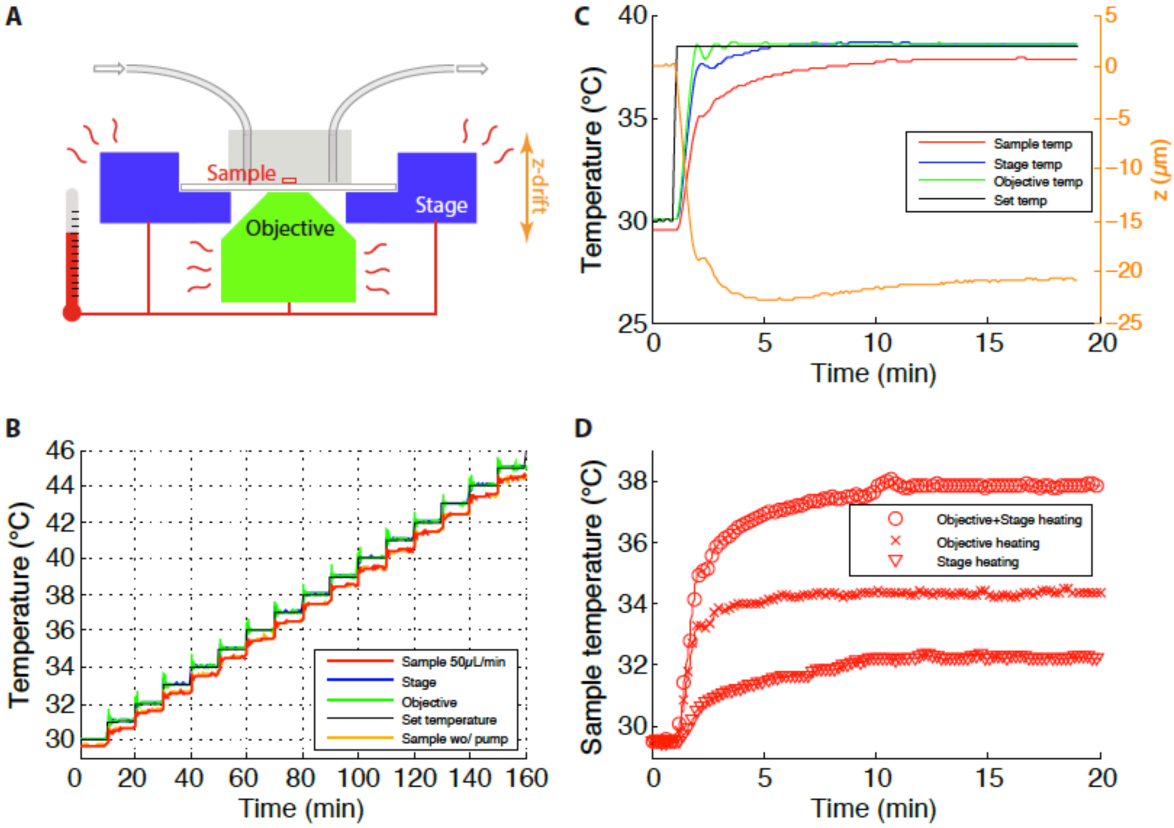

Figure S1. Sketch of the heating stage and calibration of sample temperature

(A) Sketch of the setup developed to control the sample temperature during temperature shift (TS) experiments. We built a custom sample holder (blue) with thermoelectric modules and an objective heater (green) with heating resistors. A small temperature probe was integrated into the chip to measure the actual temperature sensed by the cells. (B) Temperature calibration curves. The stage and objective temperatures follow the set temperature. The sample temperature was determined to be 0.5°C below the set temperature over the range 30°C to 45°C. This difference was independent of media flow through the device. (C) Kinetics of temperature change during TS from 30°C to 38°C. Line colors are as indicated for (B) except the orange curve displays the drift in sample z-position following the change in temperature. Curves represent the means of 5 independent experiments. (D) Comparison of different heating methods to achieve a TS from 30°C to 38°C. Both stage and objective heating is necessary to ensure a reliable sample temperature.

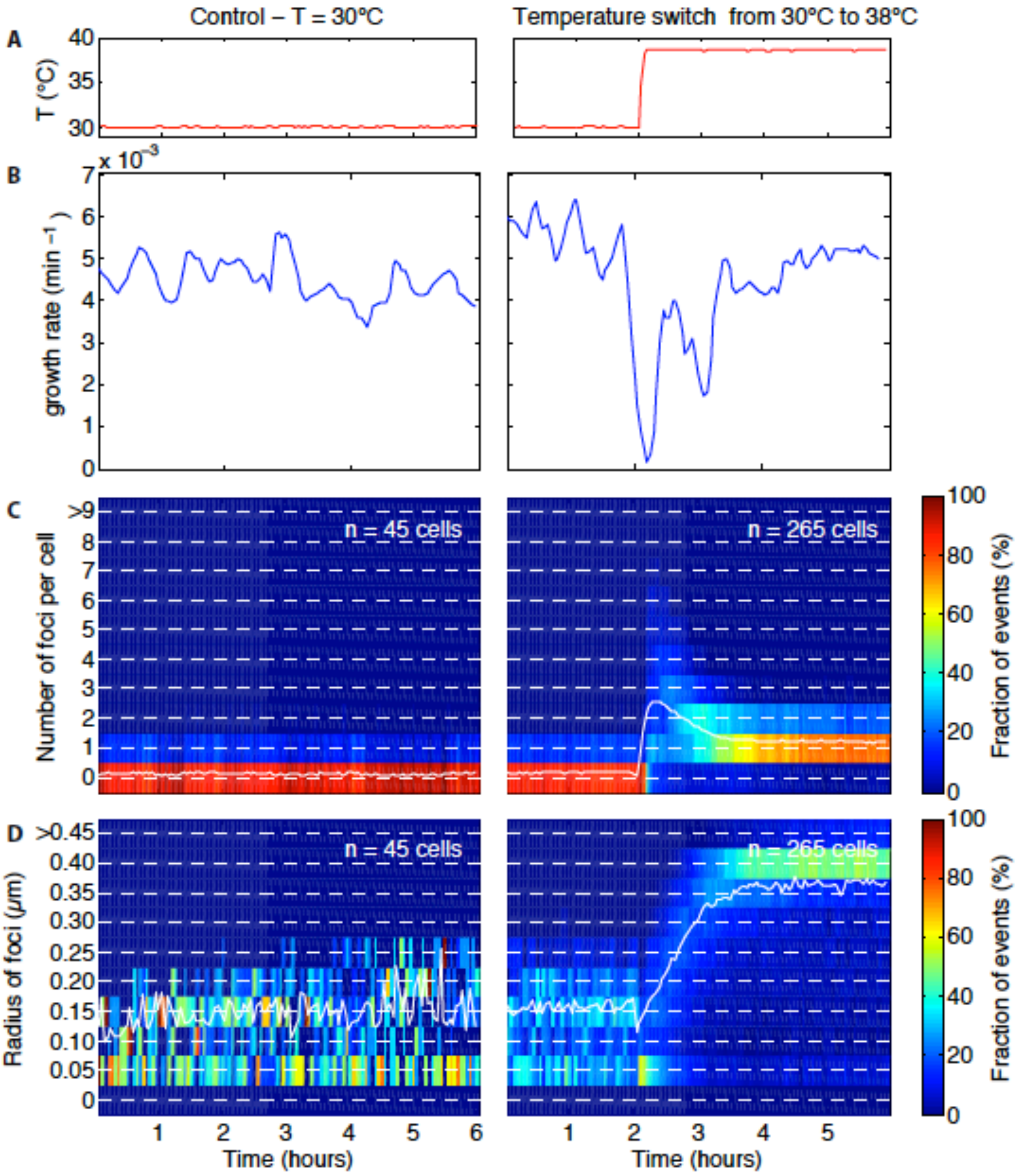

Figure S2. Comparison of foci induction and growth at 30°C and 38°C

(A) Recorded temperature of the stage. (B*)* Growth rate of the cell cluster. Growth rate is constant at 30°C (left) but decreases immediately after the TS to 38°C before recovering ~2 h later (right). (C) 2D histogram of the evolution of foci number per cell with time. The white line represents the mean value for the indicated number of cells. At 30°C, cells contain very few foci; mean = 0.2 foci/cell (left). This confirms that the illumination conditions do not artificially induce foci formation. (D) 2D histogram of the evolution of foci radius with time. The white line represents the mean value for the indicated number of cells. Foci do not grow over the course of the experiment at 30°C (left), whereas the foci size increases rapidly after the TS (right).

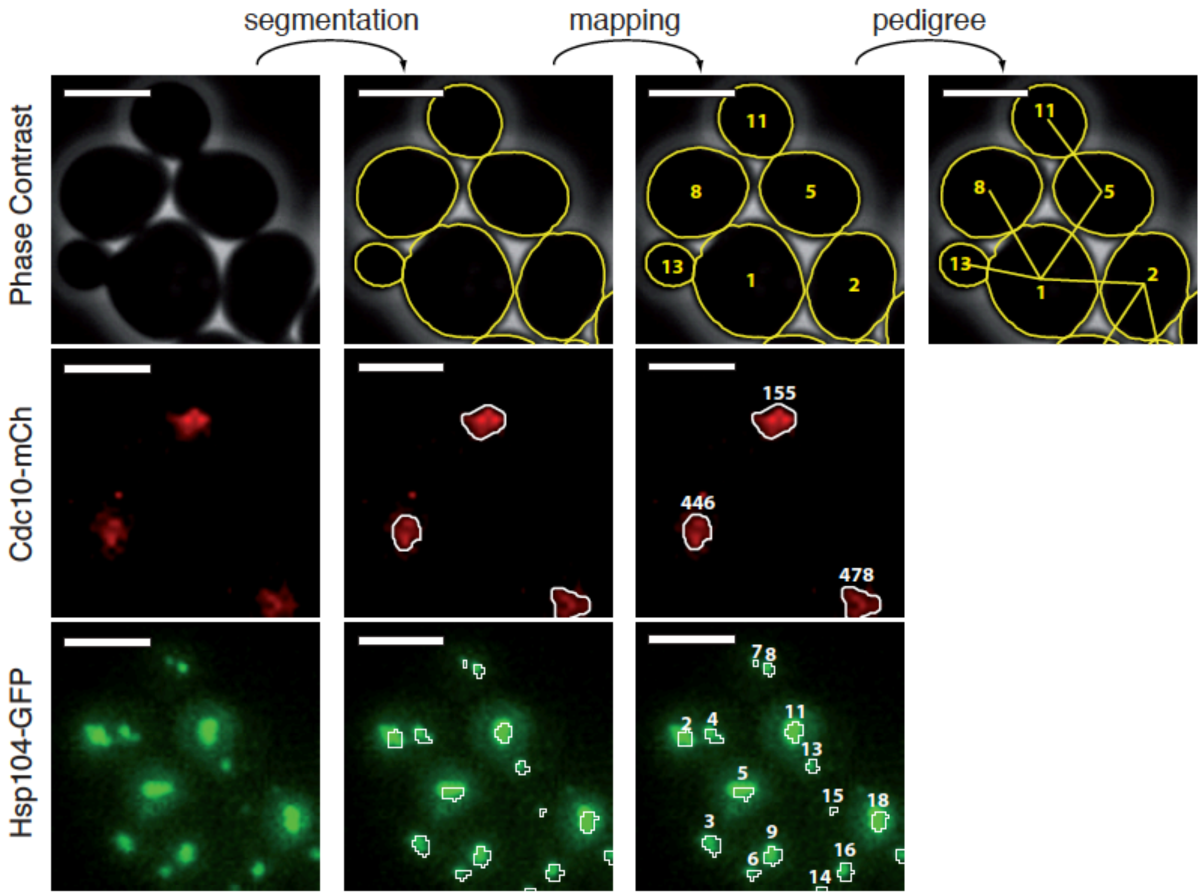

Figure S3. Image analysis pipeline

Cells (phase contrast channel), bud neck (mCherry channel), and foci (GFP channel) were automatically segmented and mapped over time by a custom-made routine. This allowed us to quantify foci features (size, number, fluorescence level), document division, follow individual cells temporally and perform pedigree analysis. The scale bar represents 4 microns.

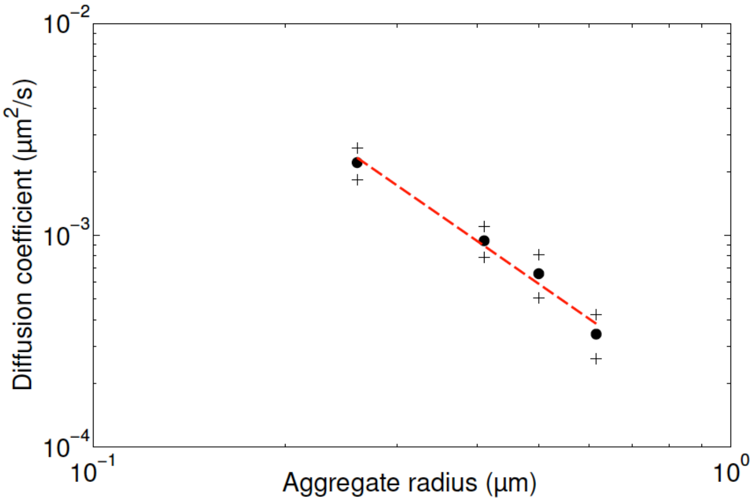

Figure S4. Aggregate diffusion coefficient as a function of size

The coefficient of diffusion of protein aggregates (PAs) was measured using standard mean square displacement analysis of PAs induced by TS. Images were acquired every 30 s using a confocal microscope to obtain a reliable estimate. The log-log plot displays a slope of -2.1, which differs from the classical Stokes-Einstein equation (Text S1).

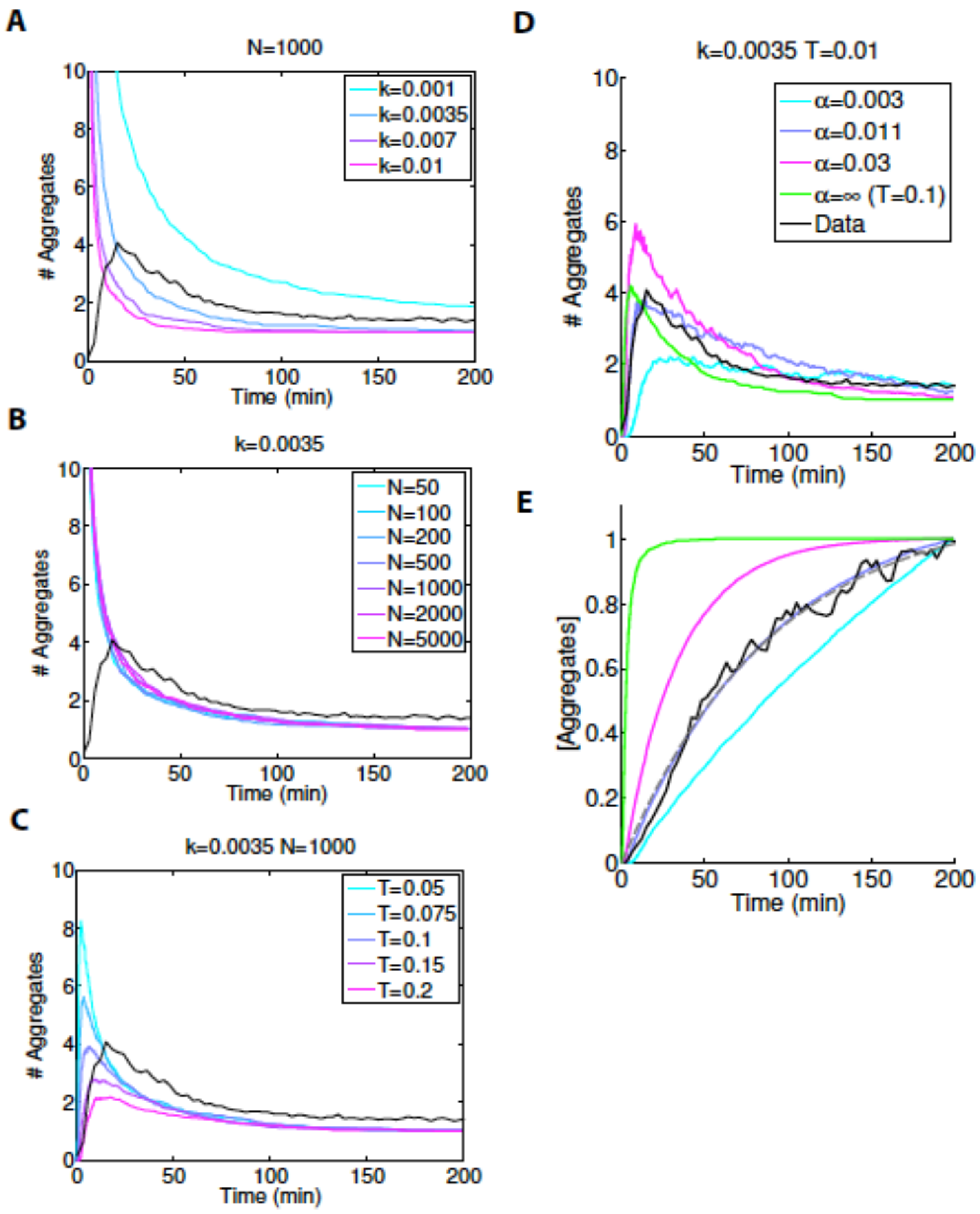

Figure S5. Effect of parameter values on the kinetics of aggregation

(A) Number of aggregates as a function of time according to the simulation described in Text S1. Each colored line corresponds to the number of PAs at the indicated value of the aggregation rate k (min^{-1}) obtained by averaging 50 runs to filter out statistical fluctuations. N is the number of initial unfolded proteins used in the simulation. The black line indicates the experimental data for the mean ± SEM number of PAs versus time observed for large mother cells (refers to Fig. 2L in the main text). (B)

Same simulation as in (A), but varying the number of initial unfolded proteins N between 50 and 5000 with a fixed value of k = 0.0035 min^{-1}. (C) Same simulation as in (A), but following the introduction of a visibility threshold T. (D, E) Same simulation as in (C), but assuming that formation of unfolded proteins follows zeroth-order kinetics with an exponential decay rate α. The number of PAs is shown in (D) and the normalized PA concentration is shown in (E). The dashed line in (E) represents an exponential fit to the experimental data (solid black line), which was used to extract the value of α.

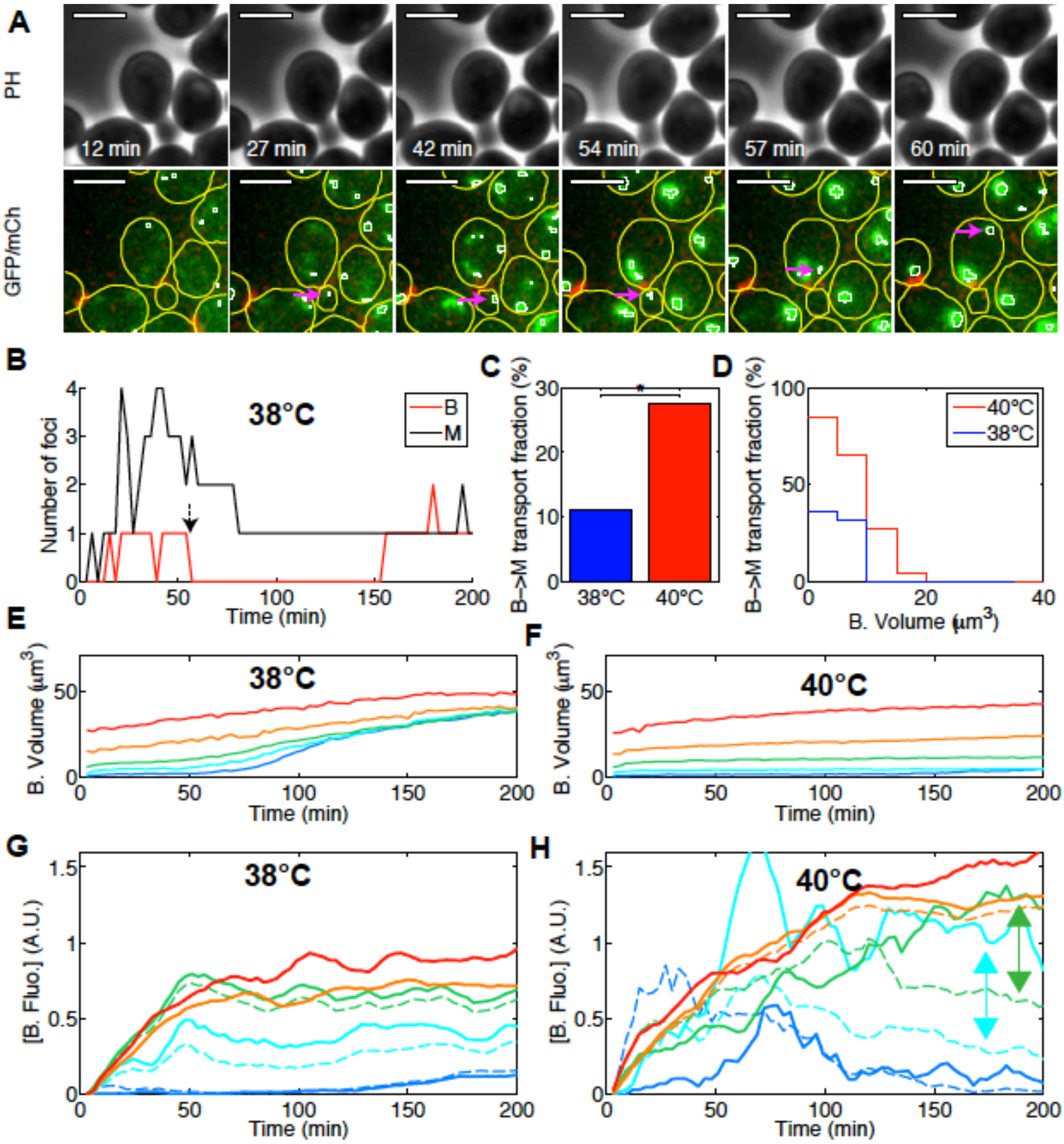

Figure S6. Bud to mother transport of aggregates

(A) Image sequence (phase contrast, overlaid Hsp104-GFP and Cdc10-mCherry fluorescence) acquired at the indicated time-points. Yellow and white lines indicate contours of the cells and Hsp104-GFP foci, respectively. Scale bar: 4 μm. Pink arrows indicate the transport of a PA from a bud to its mother. (B) Quantification of the number of foci as a function of time for the mother (M) /bud (B) pair displayed in (A). The dashed arrow indicate the time at which a transport event occurs. (C) Fraction of cells in which a transport from bud to mother (B→M) occurs during the course of the experiment at different temperature. (D) Fraction of cells with B→M transport as a function of initial bud volume. (E, F) Evolution with time of bud volume at indicated temperatures. Each colored line represents a group of individual time traces of mother-bud pairs grouped according to the initial bud volume v : v< 2 μm^3 (blue), 2 <v< 5 μm^3 (cyan), 5 <v< 10 μm^3 (green), 10 <v< 20 μm^3 (orange), v> 20 μm^3 (red). (G,H) Evolution of PA concentration in the buds with time. Color coding is as in (E,F). Solid (resp. dashed) lines correspond to groups of cells after (resp. without) removing cells in which a B→M event occurred.

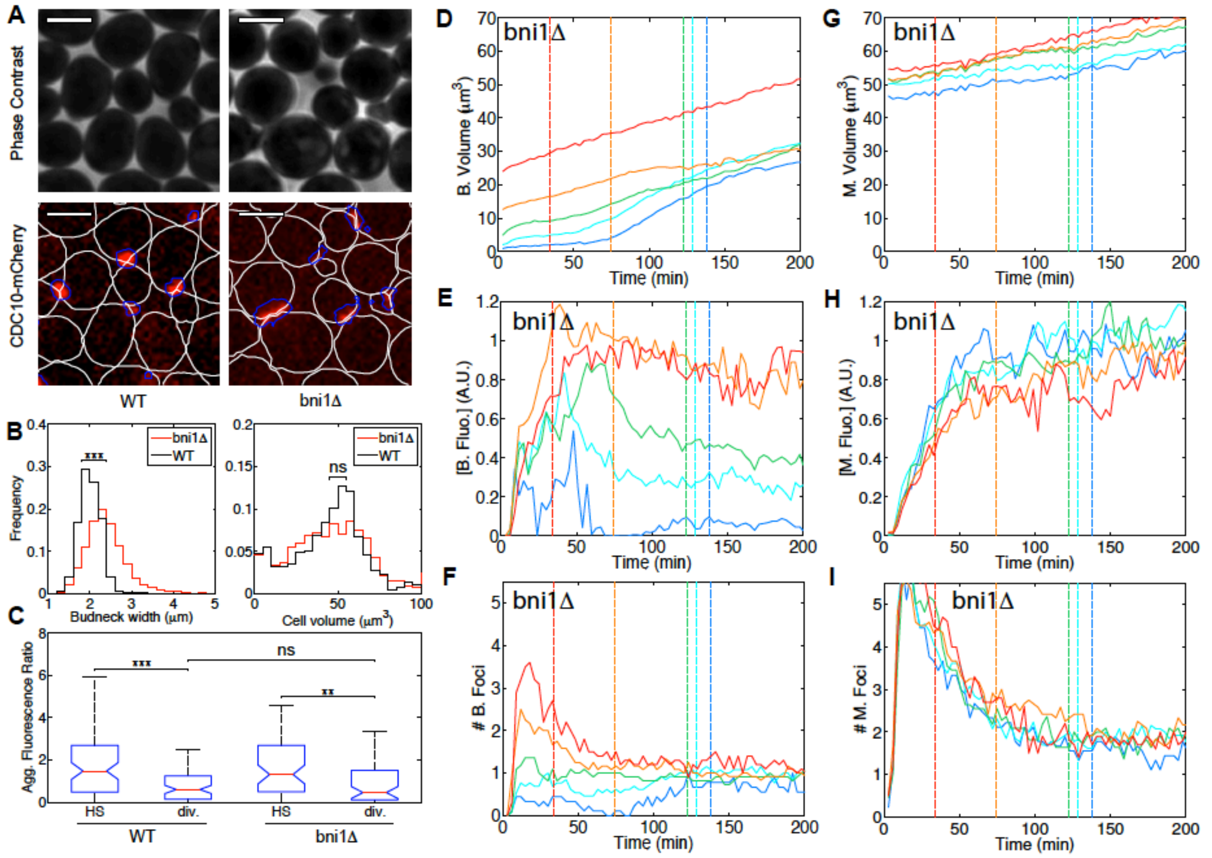

Figure S7. Asymmetric partitioning of PAs in *bni1* mutants

(A) Representative images (phase contrast and CDC10-mCherry fluorescence) of wildtype (WT, left) and *bni1*Δ (right) cells. Scale bar: 4 µm. The white lines indicate cell contours and the blue lines represent the result of bud neck segmentation (B) Left: quantification of the bud neck width following bud neck segmentation with the CDC10-mCherry marker. *Bni1*Δ mutants (red line, $n = 3241$ cells) display a 20% larger median bud neck width compared with WT cells (black line, $n = 1080$) ($p < 10^{-5}$). Right: quantification of cell size in *bni1*Δ (red line) and WT (black line) cells, indicating an insignificant difference in cell size ($p = 0.89$). (C) Comparison of the ratio of PA fluorescence in WT and *bni1*Δ mutants 12 minutes after TS and at division (div). There is no significant difference between fluorescence ratio in the mutant and WT at division. Both strains display a significant enrichment in buds between TS and division. (D-I) Evolution with time of: cell size (D, G), fluorescence concentration (E, H), and number of aggregates (foci) per cell (F, I) for the bud (left column) and the corresponding mother (right column). Each colored line represents a group of individual time traces of mother-bud pairs grouped according to the initial bud volume v : v< 2 μm^3 (blue), 2 <v< 5 μm^3 (cyan), 5 <v< 10 μm^3 (green), 10 <v< 20 μm^3 (orange), v> 20 μm^3 (red). Total number of cells analyzed = 65.

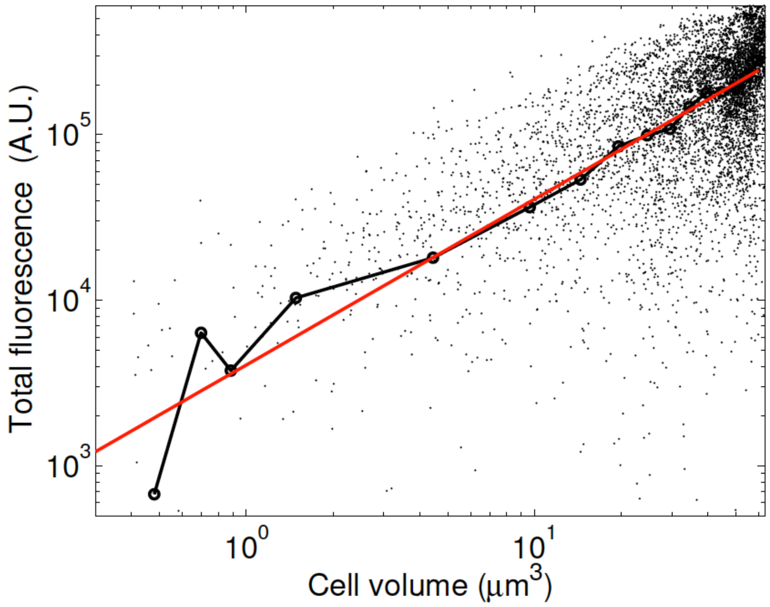

Figure S8. Scaling of fluorescence with cellular volume

Total cytoplasmic Hsp104-GFP fluorescence (sum of pixel intensities after background subtraction) within cellular compartments (including small buds) at 30°C (i.e., in the absence of foci) as a function of the volume of the compartment was calculated using the formula described in material and methods. Each point corresponds to a single cell. The solid black line represents the same data after size binning over 10 cells. The red line is a fit to the data using a powerlaw : $y=k\ x^p$ with p=1.01, indicating that normalization by cell volume is appropriate to provide a reliable estimate of concentration in cell compartments the volume of which spans several order of magnitude.

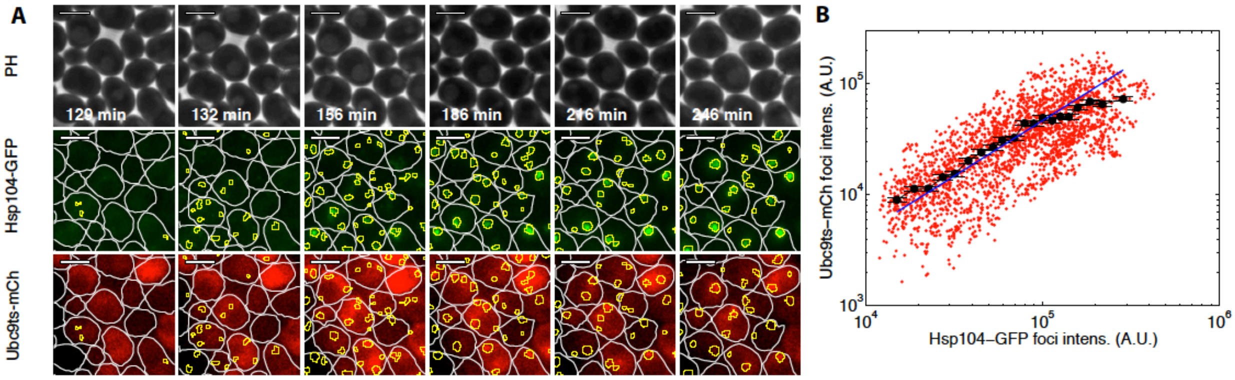

Figure S9. Scaling of Hsp104-GFP fluorescence with aggregate size

(A) Sequence of time lapse images showing the formation Hsp104-GFP and Ubc9^{ts}-mCherry foci following a temperature shift to 38°C (at t=120min). See material and methods for detailed experimental procedures. The white lines indicate cell contours. The yellow contours correspond to Hsp104-GFP foci segmentation and allow one to qualitatively assess the colocalization of Hsp104-GFP with Ubc9^{ts}-mCherry. The scale bar represents 4 microns. (B) Quantification of the linearity between protein aggregation (monitored using the Ubc9^{ts}-mCherry marker) and Hsp104-GFP level. Each red dot represents the total intensity of a single focus (n >1000 foci quantified) in GFP and mCherry channels. The black dots represent binned data (over 50 points) and error bars indicate standard error on mean. The blue line represents a linear fit to the data (y = K x).

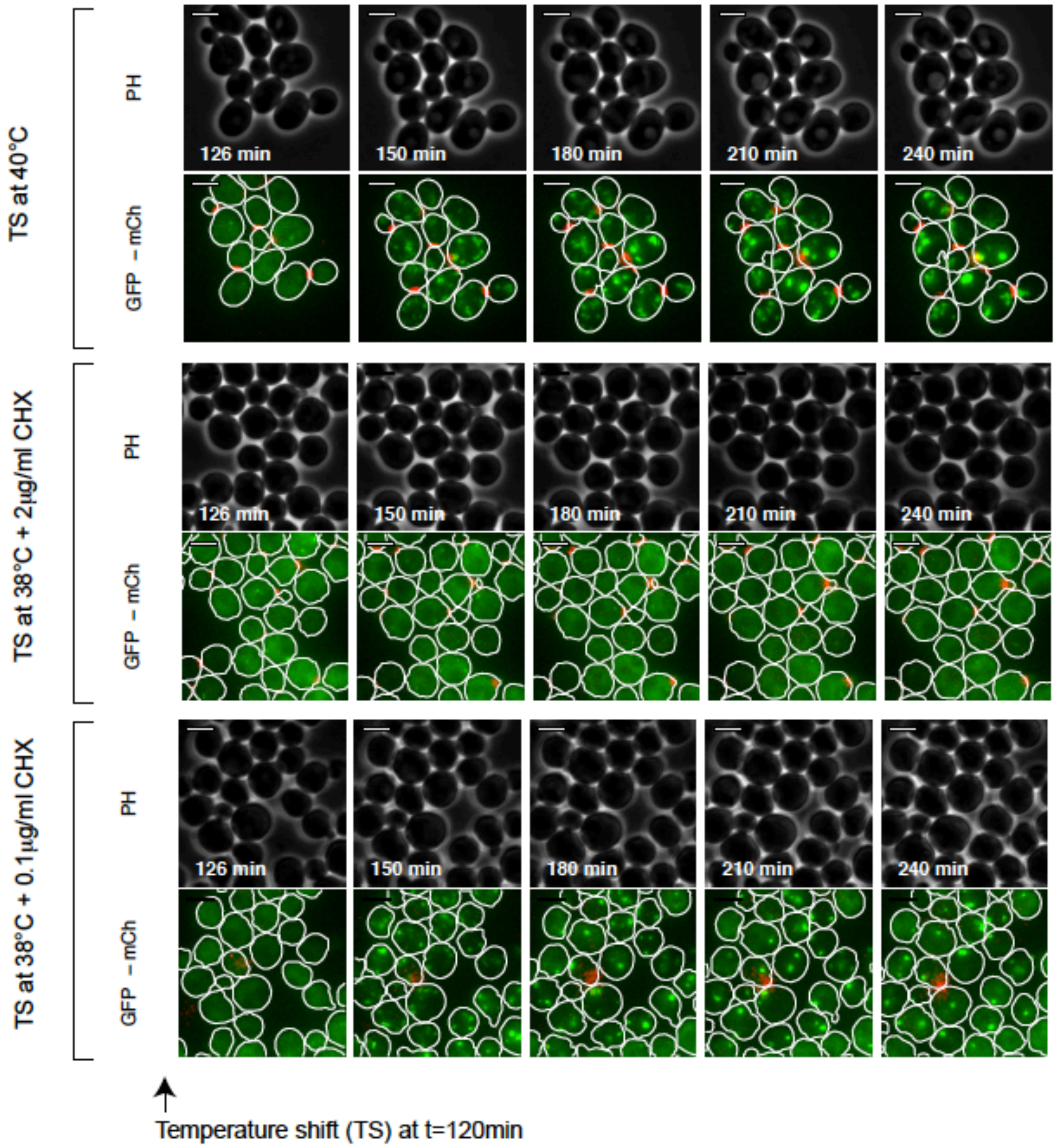

Figure S10. Perturbation of bud growth and kinetics of formation of PA

Sequence of phase contrast (PH), Hsp104-GFP and Cdc10-mCherry fluorescent images of cells following a temperature shift in the indicated conditions. The temperature shift was achieved 120 min after loading cells in the chip. White lines represent cell contours. Scale bar: 4 µm.